ADVANCED MATERIALS
www.advmat.de

Inducing Single Spin-Polarized Flat Bands in Monolayer Graphene

Matteo Jugovac, Iulia Cojocariu, Jaime Sánchez-Barriga, Pierluigi Gargiani, Manuel Valvidares, Vitaliy Feyer, Stefan Blügel, Gustav Bihlmayer, and Paolo Perna**

Due to the fundamental and technological implications in driving the appearance of non-trivial, exotic topological spin textures and emerging symmetry-broken phases, flat electronic bands in 2D materials, including graphene, are nowadays a relevant topic in the field of spintronics. Here, via europium doping, single spin-polarized bands are generated in monolayer graphene supported by the Co(0001) surface. The doping is controlled by Eu positioning, allowing for the formation of a $\bar{K}$-valley localized single spin-polarized low-dispersive parabolic band close to the Fermi energy when Eu is on top, and of a π^* flat band with single spin character when Eu is intercalated underneath graphene. In the latter case, Eu also induces a bandgap opening at the Dirac point while the Eu 4*f* states act as a spin filter, splitting the π band into two spin-polarized branches. The generation of flat bands with single spin character, as revealed by the spin- and angle-resolved photoemission spectroscopy (ARPES) experiments, complemented by density functional theory (DFT) calculations, opens up new pathways toward the realization of spintronic devices exploiting such novel exotic electronic and magnetic states.

1. Introduction

The realization of topological electronic flattened bands near or at the Fermi level is a promising route for achieving novel exotic electronic and magnetic states.[1–3] A nearly dispersionless (flat) energy band in a relevant portion of the Brillouin zone produces an electronic instability (due to the divergence of the density of states) that can determine the opening of a bandgap near the Fermi energy (E_F) and drive to new symmetry breaking ground states.[4,5] This has been so far realized by exploiting van der Waals heterostructures[6–9] and bilayer graphene,[10–12] in which, by acting on the twist angle, the electronic properties of the heterostructure can be efficiently tuned. Importantly, these flat bands typically exhibit insulating phases at half-filling, consistent with a Mott-like insulator state that can arise from electrons localized in the moiré superlattice.[11] Among the main characteristics of the flat band is the easy electrical tunability that enables access to exotic correlated phases, such as unconventional superconductivity, quantum phases, and insulating topological states, in two-dimensional platforms and without a magnetic field,[1–3] as well as orbital magnetic states,[13] potentially providing quantum anomalous Hall effect (QAHE).[14]

M. Jugovac, I. Cojocariu
Elettra – Sincrotrone Trieste
S.S. 14 – km 163.5, Basovizza, 34149 Trieste, Italy
E-mail: matteo.jugovac@elettra.eu

I. Cojocariu, V. Feyer
Peter Grünberg Institute (PGI-6)
Forschungszentrum Jülich GmbH
52425 Jülich, Germany

J. Sánchez-Barriga
Helmholtz-Zentrum Berlin für Materialien und Energie
Elektronenspeicherring BESSY II
Albert-Einstein-Str. 15, 12489 Berlin, Germany

J. Sánchez-Barriga, P. Perna
IMDEA Nanociencia
Campus de Cantoblanco
c/ Faraday 9, 28049 Madrid, Spain
E-mail: paolo.perna@imdea.org

P. Gargiani, M. Valvidares
ALBA Synchrotron Light Source
08290 Barcelona, Spain

S. Blügel, G. Bihlmayer
Peter Grünberg Institut and Institute for Advanced Simulation
Forschungszentrum Jülich and JARA
52425 Jülich, Germany

I. Cojocariu
Dipartimento di Fisica
Università degli studi di Trieste
Via A. Valerio 2, 34127 Trieste, Italy

The ORCID identification number(s) for the author(s) of this article can be found under https://doi.org/10.1002/adma.202301441

DOI: 10.1002/adma.202301441

Flat bands driven by electronic correlations are expected to develop in monolayer graphene when doped to the van Hove singularity.[15,16] By over-doping the quasi-freestanding monolayer of graphene via metal intercalation, the van Hove singularity can be shifted to E_F,[17–19] enabling access to exotic ordered ground states in transport. Flat bands are generally challenging to engineer, and having them spin-polarized is critically essential for developing unconventional electronic devices whose multiple new functionalities exploit the spin degrees of freedom rather than the charge.[20,21] An alternative route to build flat bands in monolayer graphene (Gr) is to resort to the spin–orbit coupling (SOC) effect induced by the proximity with magnetic and/or heavy-metal layers. Gr/3d-ferromagnets (Gr/3d-FM) and Gr/4f-materials enclose, in fact, remarkable technological opportunities by bridging spintronics with ultrafast Gr-based electronics and photonics.[22–24]

Among Gr/3d-FM, Gr/Co structures deposited onto heavy metals (HMs) have been proposed for the realization of novel spin–orbitronics devices because of their enhanced perpendicular magnetic anisotropy[25–28] and sizeable Dzyaloshinskii–Moriya interaction, allowing for increased thermal stability, stabilization of chiral spin textures, and extrinsic (Rashba) SOC.[29–31] Moreover, the heavily hybridized Gr bands trigger the spin-dependent transport of Gr/Co.[32]

While the main drawback in Gr/3d-FM systems is that the strong hybridization impacts the Gr electronic properties leading to an energy downshift of the Dirac cone, Gr/4f-FM interfaces present a weak interaction that preserves graphene's electronic structure.[33] On the other side, Gr-spaced magnetic systems with antiferromagnetic exchange-coupling offer additional exciting opportunities for spintronic applications and magnetic information storage,[34] potentially outperforming the commonly used in-plane synthetic ferrimagnetic and antiferromagnetic spin valve structures.[35] In this context, the possibility of establishing routes toward this goal by merging appealing magnetic properties of 3d- and 4f-FM with Gr unique electronic, mechanical, and thermal properties appears highly relevant.

In this work, by means of spin-resolved ARPES experiments combined with DFT calculations, we investigate the role of europium in modifying the spin-dependent electronic properties of monolayer Gr on Co(0001). Manifold effects are revealed: i) an enhancement of the charge transfer into Gr via Eu doping; ii) the existence of a spin-polarized Gr-Co hybrid state formed by positioning Eu on top or beneath the Gr monolayer, in both cases with a single spin (majority) character. While in the former case, the low-dispersive parabolic Gr-Co hybrid band is observed close to Fermi energy, extending all over the surface Brillouin zone (SBZ), when Eu is intercalated, the π^* band becomes flat; iii) the large exchange coupling due to the presence of Eu induces the splitting of the π band that crosses the 4f states into minority and majority branches bending toward higher and lower binding energies respectively, accompanied by a bandgap opening at the Dirac point of ≈0.36 eV. Our findings demonstrate the relevance of using Eu for efficiently tuning the Gr electronic properties and driving the interlayer magnetic coupling.

2. Results

2.1. Structural and Electronic Properties

The Gr/Co interface was grown by in situ chemical vapor deposition (CVD) synthesis on top of a 10 nm thick Co(0001) film grown on W(110), following an established procedure.[36–38] **Figure 1** shows the low-energy electron diffraction (LEED) and ARPES measurements of the three structures investigated. Left, central, and right panels present the case of pristine Gr/Co, Eu on Gr/Co, and Gr/Eu/Co, respectively.

First, by inspecting the LEED patterns in the top panels, we immediately observe the transition from a (1×1) LEED reconstruction in the case of the strongly interacting Gr/Co(0001) to the $\sqrt{3}\times\sqrt{3}$ R30° structure found in both on-top and intercalated Eu systems. We also notice that, while in pristine Gr/Co, and in Eu/Gr/Co, graphene is strained by 1.7% (Co/Gr lattice parameters = 2.507/2.465 Å), europium intercalation leads to a quasi-freestanding graphene, where the strain in Gr is almost completely lifted (strain factor of 0.1%).

The electronic structure near the Fermi level of the three systems, plotted in Figure 1a–c, resembles the above-discussed structural order of the respective LEED patterns. Evident changes in the appearance of the Fermi surfaces (FS) reflect the presence of Eu and its location at the Gr/metal interface. The FS of pristine Gr/Co is dominated by six intense features located at the $\bar{K}$ point of the SBZ, assigned to emission from the minicone states.[37] In the case of on-top europium, the strain, the $\sqrt{3}\times\sqrt{3}$ R30° surface reconstruction, as well as the charge transfer imposed by the presence of on-top Eu, contribute to the appearance of Umklapp scattering-induced Alhambra-style mosaics (Figure 1b). The charge transfer also leads to the observation of new states at the $\bar{K}$ point, discussed in the following. The FS of the Eu-intercalated structure in Figure 1f deserves particular attention. In fact, we can clearly see the emergence of flat bands over the whole SBZ from $\bar{K}$ to $\bar{M}$. In order to deeper characterize the changes in the electronic structure of the three systems, the 2D energy versus momentum maps are presented in Figure 1d–f. The strong interaction between Gr monolayer with Co(0001) leads to the formation of two Dirac-like features, one at high binding energy (π band) and a second one in the proximity of the Fermi level (minicone), as seen in Figure 1d and its inset. As demonstrated previously[37] and reported in Figure S2 (Supporting Information), this state, which arises from the hybridization of C $2p_z$ with the Co 3d band, is characterized by a majority spin polarization along with the whole band and has its apex right at the Fermi level. The main graphene Dirac cone is found at 2.83 ± 0.04 eV and is characterized by a Fermi velocity of 0.76×10^6 m s^{-1}, consistent with the value of 0.66×10^6 m s^{-1}, obtained from previously reported DFT calculations for Gr/Co.[39]

Strong influences on the band structure distinguish the presence of Eu on top of the epitaxial Gr/Co interface, which leads to an enhanced charge transfer to the Gr layer (Figure 1b). Due to the additional periodicity, the original (1×1) primitive cell folds into the $\sqrt{3}\times\sqrt{3}$ R30° reduced zone (central panel), as previously reported for similar systems.[40] This periodicity leads to the observation of the spectral features found at $\bar{\Gamma}$ in the primitive cell at the $\bar{K}$ point of the new supercell. This is clearly visible in the

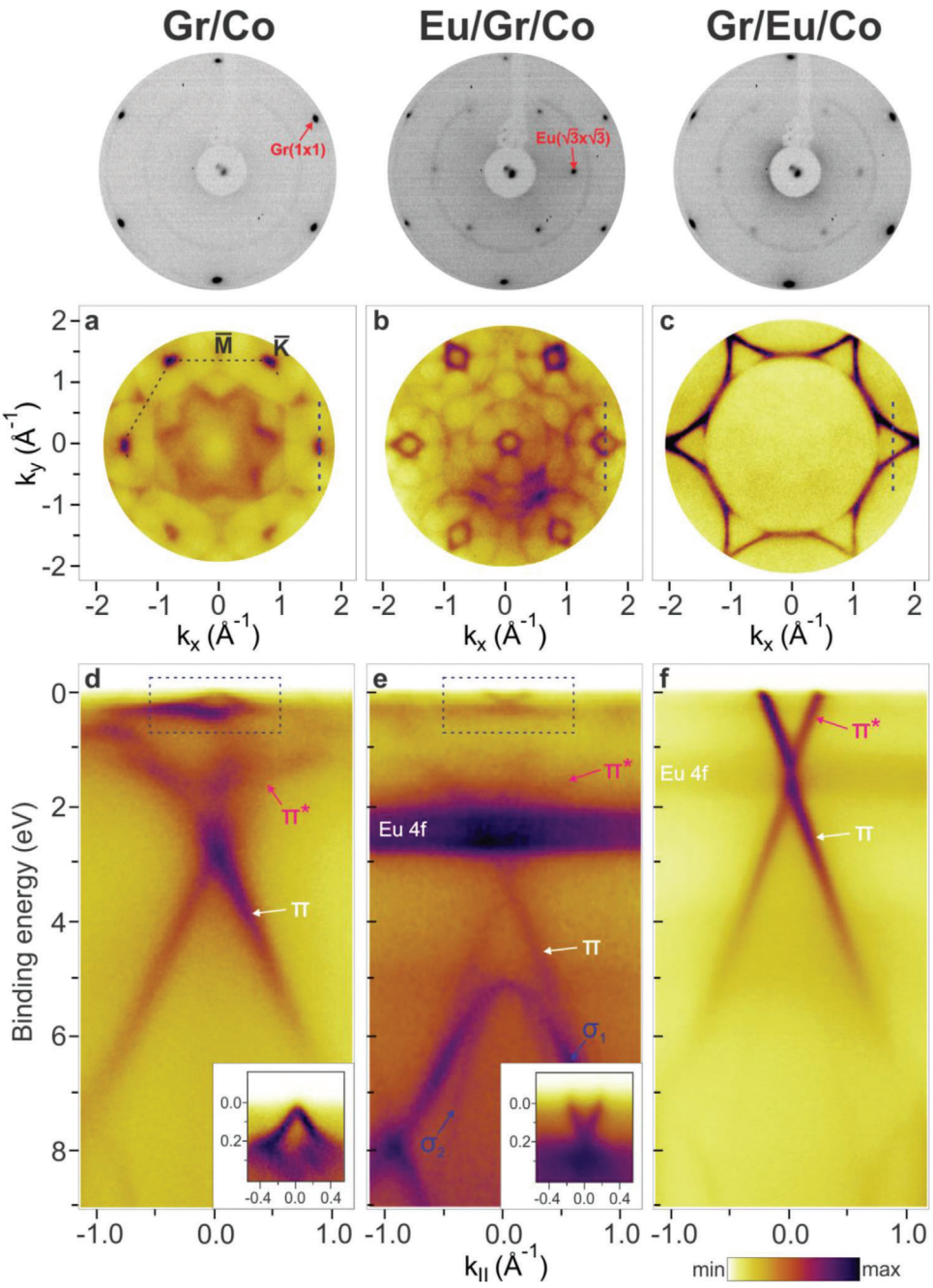

Figure 1. Landscape of the structural and electronic properties upon Eu intercalation in Gr/Co(0001). LEED patterns acquired at a kinetic energy of 69 eV (top panels) and ARPES energy vs momentum maps (d,e,f) acquired at the $\bar{K}$ point of the first Brillouin zone (along the dashed path indicated in (a)) for Gr/Co (left), Eu on Gr/Co (central), and Gr/Eu/Co (right) along with the respective Fermi surfaces acquired at 50 meV binding energy (a,b,c). The insets in (d) and (e) show a zoom on the region near the Fermi level. The measurements were acquired with vertically polarized photons of $h\nu$ = 40 eV.

momentum map acquired at the $\bar{K}$ point of the SBZ (Figure 1e), where, along with the Gr π band, the repetition of the σ dispersing bands is sizable. By fitting the linear region of the π band, the Dirac point is found at 3.15 eV binding energy, shifted by ≈0.3 eV with respect to pristine Gr/Co. The presence of metallic Eu also leads to the appearance of an intense and non-dispersive 4f band centered at ≈2.53 eV binding energy. Additionally, we note the presence of a low-dispersing state in the proximity of the Fermi level (located at the $\bar{K}$ point of the relative FS), as indicated by the blue box in Figure 1e. The magnified view of this region is shown in the inset. This low-dispersive state, found in the region between the Fermi level and ≈0.2 eV binding energy, possesses parabolic dispersion and closely resembles the band characteristics of the minicone state observed in pristine Gr/Co. By fitting its

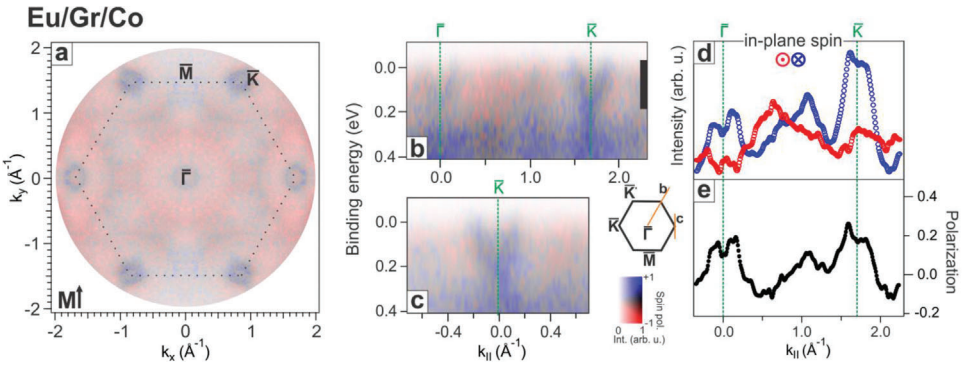

Figure 2. Spin-resolved electronic structure of the Eu/Gr/Co system. a) Spin-resolved FS (binding energy 50 meV) of the Eu/Gr/Co system. b) Spin-resolved energy versus momentum map acquired along the $\overline{\Gamma K}$ direction. c) Spin-resolved energy versus momentum map acquired at the $\bar{K}$ point. d) Spin-resolved momentum distribution curves acquired along the $\overline{\Gamma K}$ direction at the Fermi level (between 0.0 and 0.2 eV and marked by a solid black line at the right side of (b)). e) Spin polarization curve obtained by a normalized difference of the two curves in (d). According to the 2D color code on the right side of (c), blue and red intensities correspond to majority and minority electronic states.

branches in the upper, linear part of the band, we determine the crossing position to be at 0.14 eV binding energy with a Fermi velocity of 2.2×10^5 m s^{-1}, 32% higher with respect to the undoped interface.[37] This agrees well with the value of 3.0×10^5 m s^{-1} obtained by DFT calculations.

Intercalation of the topmost Eu layer at the Gr/Co interface is achieved by annealing the Eu/Gr/Co sample to 620 K. Such a temperature ensures the complete intercalation of an Eu $\sqrt{3} \times \sqrt{3}$ R30° layer at the interface and the eventual Eu excess desorption on top of the Gr layer (top right panel). The presence of Eu at the interface radically alters the band structure with respect to the Eu/Gr/Co case. The most striking difference with respect to the pristine interface is that the hybridization between Gr and Co is lifted, therefore leading to a quasi-freestanding Gr layer. This reflects in an increased Fermi velocity of the main Dirac cone (0.84×10^6 m s^{-1}) with respect to the Gr/Co undoped interface, consistent with the value of 0.95×10^6 m s^{-1} obtained by DFT. Nevertheless, the presence of Eu at the interface leads to the n-doping of the Gr layer due to charge transfer, downshifting the Dirac point to 1.55 eV (Figure 1c) and inducing the occupancy of the π^* Gr band. Upon intercalation, the direct interaction of Eu with the Co substrate induces a shift to lower binding energies of the Eu 4f bands, being now centered at 1.49 eV binding energy.

2.2. Spin-Resolved Electronic Structures

The spin character determination of the Gr bands in the three considered cases is based on spin-resolved momentum mapping.

In the case of Eu on top of Gr, the spin-resolved FS, reported in **Figure 2**a, is dominated by the low-dispersive states at the $\bar{K}$ point of the SBZ, possessing an in-plane sixfold symmetry. These bands have predominately spin majority character (see Figure 2b,c). Interestingly, the superstructure originating from the ordered Eu layer on top of Gr leads to the observation of these spin-polarized bands also at the $\bar{\Gamma}$ point of the SBZ (Figure 2b). The character of these bands is further analyzed in the spin polarization plots shown in Figure 2d,e. The majority and minority plots, acquired in the region near the Fermi level along the $\overline{\Gamma K}$ direction, highlight the occurrence of these features only in the majority channel, both at $\bar{K}$ and $\bar{\Gamma}$ points of the SBZ. Therefore, these low-dispersive parabolic bands own single spin character, in very good agreement with the DFT simulations shown below. Moreover, we note that the parabolic band lies above the non-dispersive Co 3d band, centered at ≈0.3 eV binding energy, which is also well known to be majority spin polarized.

Figure 3a shows the spin-polarized FS of the Gr/Eu/Co system. In order to better visualize the flat band, the sample is tilted to include the $\bar{K}$, $\bar{M}$ and $\bar{K}'$ points in the 2D momentum map. The spin-resolved FS of this system allows us to appreciate the shape and polarization of the π^* states, which are occupied due to electron transfer from Eu. As visible in Figure 3a, the electron pockets formed by the π^* states show strong trigonal warping, as expected for Dirac cones. These states do not display a predominant spin character. In Figure 3b,c, the non-dispersive Eu 4f band is visible ≈1.49 eV binding energy and shows a predominant minority spin character. Figure 3c demonstrates that the Dirac cone bandgap opening occurs in correspondence with the Eu 4f band as a consequence of the large spin–orbit coupling. As noted before, the population of the π^* band also leads to band flattening along the $\overline{KMK'}$ direction of the SBZ. The flat π^* band, extending toward the $\bar{M}$ point, is characterized by a prevalence of the majority spin polarization, as clearly visible in the spin polarization plot on top of Figure 3d, in line with the DFT calculations shown below. From the extent of the FS, we evaluated the charge carrier density, being 2.98×10^{14} cm^{-2}.

A deeper description of the results is based on DFT+U calculations, as presented below. For the Eu/Gr/Co case, we see in **Figure 4**a that the position of the Eu 4f band (2.5 eV) matches the experimental value when a Hubbard U value of 5.9 eV is assumed. The Dirac cone of graphene can be found at 3.5 eV (notice that in the $\sqrt{3} \times \sqrt{3}$ R30° Brillouin zone, the $\bar{K}$-point of the (1×1) cell is backfolded to the $\bar{\Gamma}$ point). At the $\bar{M}$ point, one can observe a pronounced spin-splitting of the Gr band of ≈0.7 eV (shown in Figure S3a, Supporting Information). The parabolic feature at the (backfolded) $\bar{K}$ point, dominating the momentum map in Figure 2a, is here attributed to graphene. This majority band arises from the hybridization of Gr with Eu 5d- and Co 3d-states (the Eu character is covered here by the Gr one). In addition,

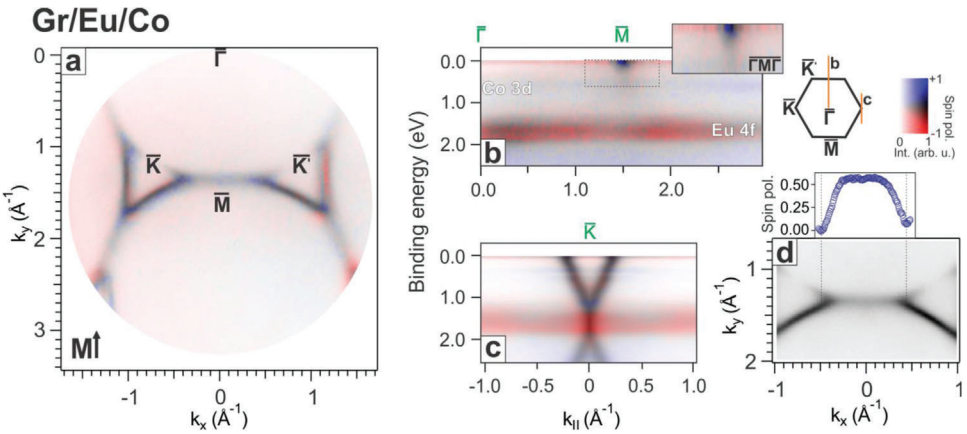

Figure 3. Spin-resolved electronic structure of the Gr/Eu/Co system. a) Spin-resolved Fermi surface (binding energy 50 meV) of the Gr/Eu/Co system. b) Spin-resolved energy versus momentum map acquired along the $\overline{\Gamma M \Gamma}$ direction. Inset shows a zoom of the area indicated by the dashed lines, where the flat band is clearly visible. c) Spin-resolved energy versus momentum map acquired at the $\bar{K}$ point. d) Momentum map of the region near the $\bar{M}$ point, along with the plot of spin polarization acquired along the flat band ($\overline{KMK'}$ direction). According to the 2D color code on top of panel d), blue and red intensities correspond to majority and minority electronic states. The measurements were performed using a photon energy of $h\nu = 65$ eV, vertical polarization.

we note that Eu and Co are coupled ferromagnetically through the Gr layer, opposite to the intercalated Eu system, in which the direct contact with cobalt induces antiferromagnetic coupling.[33] This is also confirmed by the DFT calculation performed for the Eu/Gr/Co system considering an AFM coupling between Eu and Co (Figure S4, Supporting Information), which clearly does not match the experimental bands.

The DFT calculations for the intercalated case, that is, Gr/Eu/Co reported in Figure 4b, predict the Eu 4f band at lower binding energies (1.8 eV), consistent with the experimental results presented in Figure 1e,f. A wider energy range is shown in Figure S3b (Supporting Information). The graphene Dirac point is located at 1.3 eV, where a bandgap opening occurs due to C hybridization with the Eu 4f band (as visible in Figure 3c and the scenario discussed in ref. [23] – see also the discussion below). The flat band along $\overline{KMK'}$ observed in the spin-resolved momentum map in Figure 3a is found in the DFT plot along the $\overline{\Gamma M}$ direction of the SBZ due to the $\sqrt{3} \times \sqrt{3}$ R30° periodicity of the Eu layer. This flat band appears upon occupation of the π^* states of graphene due to charge transfer (n-doping) from the Eu atoms. The π^*-derived flat band is characterized by a majority spin polarization along the whole band, in agreement with the experimental spin-resolved results of Figure 3. The spin character originates from the hybridization of Gr with the Eu d-states, which are polarized oppositely to the 4f states.

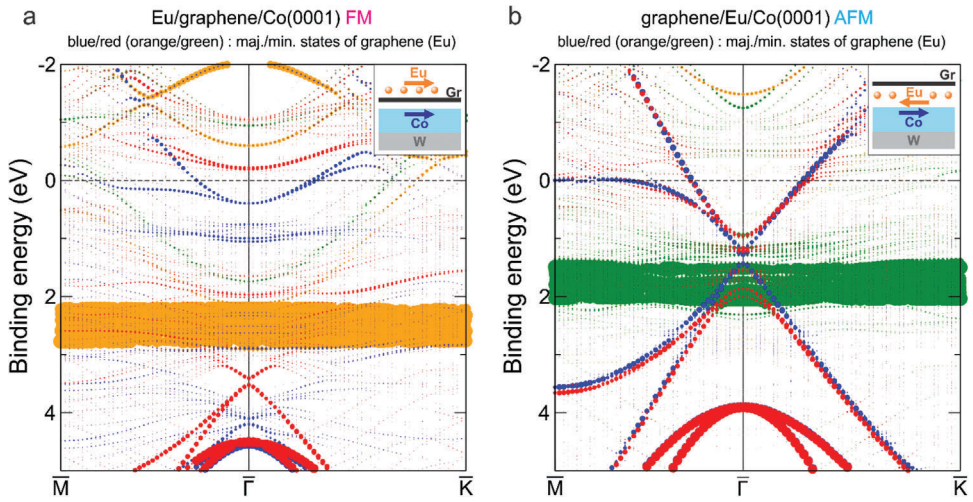

Figure 4. DFT band structures of Eu/Gr/Co and Gr/Eu/Co. The blue (red) symbols indicate the weight of graphene majority (minority) character, the yellow (green) ones Eu majority (minority) character (w.r.t. the Co magnetization). In the case of Eu/Gr/Co we see that Eu couples ferromagnetically (FM) to Co and the graphene spin-splitting follows this magnetization. In Gr/Eu/Co the coupling between Eu and Co is antiferromagnetic (AFM) and the graphene bands inherit a small spin-splitting following the Eu spin polarization. For a better alignment of the Eu 4f bands we reduced the Hubbard *U* value here to 5.9 eV.

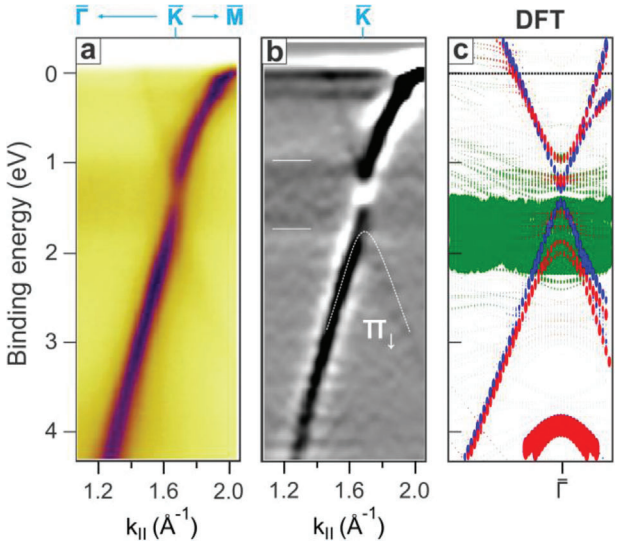

Figure 5. Bandgap opening at the Dirac point and spin filter in Gr/Eu/Co. a,b) Energy versus momentum map of the Gr/Eu/Co system acquired along the $\overline{\Gamma KM}$ direction and its second derivative plot. On the right, the minority branch of the π band is indicated by the dashed line. c) DFT zoom-in of the region presented in the experimental spectra. The color code of the simulations refers to the one in Figure 4.

We now focus on the region close to the $\bar{K}$ point of the Gr/Eu/Co system, particularly around the graphene Dirac point. In order to highlight the band features, we plot a zoom of the ARPES spectrum, along with its intensity plot in the second derivative (**Figure 5**a,b, respectively). The fit reveals that the presence of Eu at the interface induces a bandgap opening at the Dirac point of ≈0.36 eV, comparable with previous studies.[41] We underline that, due to the strong exchange coupling, the Eu 4f bands also act as a spin filter, splitting the π band that crosses the Eu 4f states into two branches, with the minority part bending toward higher binding energies, as perfectly confirmed by the zoom-in of the DFT simulation (Figure 5c).

3. Conclusion

We have engineered a spin-polarized flat band in quasi-free standing monolayer graphene by exploiting doping, induced SOC, and magnetic coupling. The unique electronic, mechanical, and thermal properties of graphene merged with interfacial interactions, such as those provided by 3d and 4f metals, offer an ideal, easily accessible, fruitful platform for experimentally realizing exotic quantum ground states. The europium doping of the graphene/cobalt interface leads to a fully tunable system in terms of electronic and magnetic properties. Depending on the europium position at the interface, a manifold appearance of different effects occurs. Cobalt-graphene hybridization is preserved when europium is on top, with the formation of a $\bar{K}$ valley localized, low-dispersive, single spin-polarized parabolic band close to the Fermi level due to the charge transfer induced to the conduction band states. While, in this case, cobalt and europium are ferromagnetically coupled, intercalation of the rare-earth leads to antiferromagnetic coupling. As a result, the n-doped graphene layer exhibits a quasi-freestanding electronic structure featuring a bandgap opening at the Dirac point. The europium 4f band acts as a spin filter for the graphene π states, allowing for the channeling of graphene bands with opposite spin characters. Furthermore, the emergence of a highly localized π^* flat band at the $\bar{M}$ point of the surface Brillouin zone is observed and displays a single spin character along the whole band. The combination of these unique spin features offers a multifaceted platform for spintronics.

4. Experimental Section

Sample Preparation: The substrate for the experiment was a W(110) single crystal. The cleaning procedure consisted of repeated annealing cycles up to 1370 K in 3×10^{-7} mbar of molecular oxygen, followed by high-temperature flashes in ultrahigh vacuum (UHV) up to 2200 K until a sharp (1×1) LEED pattern was obtained. Cobalt was deposited from a 99.995% purity Co rod using an e-beam evaporator while keeping the W(110) crystal at room temperature. A total of 50 ML (10 nm) Co was deposited at a rate of ≈2.3 Å min^{-1}. After deposition, the structural quality and cleanliness of the film were checked by LEED and X-ray photoelectron spectroscopy (XPS), respectively.

Graphene growth was performed by exposing the Co film to ethylene (C_2H_4) partial pressure of 5×10^{-7} mbar, following a well-established recipe.[36–38] In all the experiments, the base pressure of the preparation and analysis chambers was below 2×10^{-10} mbar.

Europium was evaporated at a rate of 0.65 Å min^{-1} from a homemade cell while keeping the sample at room temperature until a saturated layer in $\sqrt{3} \times \sqrt{3}$ R30° arrangement is formed. In order to intercalate the topmost Eu layer at the Gr/Co interface, the Eu/Gr/Co sample was annealed to 620 K. The temperature was measured using a K-type thermocouple.

Instrumentation: Spin-integrated and -resolved ARPES measurements were carried out at the NanoESCA beamline of Elettra synchrotron in Trieste (Italy), using a photoemission microscope (PEEM) operating in reciprocal space mode (k-PEEM).[42] The sample is illuminated with soft X-rays from the beamline equipped with two Apple-II type undulators, allowing for obtaining over a range from 40 to 1300 eV with variable polarizations: linear horizontal, linear vertical, or elliptical. The kinetic energy of the photoelectrons is selected by applying a proper bias voltage to the sample. The photoemitted electrons are collected by an optical column, energy-filtered in the double-hemispherical configuration (IDEA), and finally projected onto a 2D detector. In addition, the spin-dependent reflectivity of a W(001) target inserted in the optical column allows performing real or reciprocal space imaging with in-plane spin resolution. The quantification of the spin polarization can be performed by considering constant the spin sensitivity, being 0.42 and 0.05 for the two employed scattering energies.[43] Therefore, the spin polarization P can be given in an interval ranging from −100% (fully spin-down) to +100% (fully spin-up). Prior to spin-resolved measurements, the sample was in situ magnetized using a magnetic field of ≈0.5 T, sufficient to align the Co magnetic domains along the easy magnetization axis of the W(110) crystal.[44] During the measurements, the sample was kept at liquid nitrogen temperature. The mapping of the electronic structure was performed using p-polarized incoming light with photon energy 40 eV (if not stated differently).

Theoretical Simulations: DFT was employed in the generalized gradient approximation[45] using van der Waals corrections in the D3 form.[46] The calculations were performed with the full-potential linearized augmented planewave method in thin-film geometry[47] as implemented in the Fleur code.[48] To describe the Eu 4f electrons, a Hubbard U of 6.9 eV and $J = 0.9$ eV unless noted otherwise was included. However, for the comparison of the simulations to the experimental band structure, $U = 5.9$, $J = 0.9$ eV gives a better agreement. Despite that, small variations of U do not affect the structure or magnetic ordering.[33] For the Gr/Eu/Co system, a setup according to previous studies is assumed,[33] that is, a $\sqrt{3} \times \sqrt{3}$ unit cell with seven layers of Co(0001) and a Eu atom in hcp position that is covered with graphene. The relaxed Eu-graphene distance

is 2.56 Å while the Eu/Co distance is 2.49 Å, Eu is coupled antiferromagnetically to Co. In the Eu/Gr/Co system again a $\sqrt{3} \times \sqrt{3}$ unit cell was assumed and graphene is 2.10 Å above Co in top-fcc adsorption geometry. Eu prefers the hollow site 2.52 Å above graphene and the ferromagnetic coupling to Co was found to be 0.05 eV more favorable than an antiferromagnetic one. In the Gr/Eu/Co system, the DFT-derived total magnetization provides for Eu −6.98 μ_B, while the interface Co has 1.64 μ_B, and the sub-interface one has 1.67 μ_B. For the Eu/Gr/Co case, the values are 6.99, 1.61, and 1.70 μ_B, respectively. These moments are found within a radius of 1.40 (1.17) Å around the Eu (Co) positions. 98% of the Eu moments come from the 4f states. The values of magnetic moments are consistent with previous reports.[33] Spin–orbit coupling (SOC) was included self-consistently in the band structure calculations. An in-plane SOC would lead to the breaking of the hexagonal symmetry of the Brillouin zone, as the experimental images average over all $\bar{M}$ and $\bar{K}$ directions an out-of-plane spin-quantization axis was chosen to keep the symmetry. In all cases, an in-plane Co lattice constant of 2.51 Å was used. The optimized structure is displayed in Figure S5 (Supporting Information).

Supporting Information

Supporting Information is available from the Wiley Online Library or from the author.

Acknowledgements

This research is supported by the FLAG-ERA grant SOgraphMEM Project PCI2019-111867-2 and PCI2019-111908-2 by Spanish AEI and by German DFG. IMDEA team acknowledges support by the Regional Government of Madrid through Project P2018/NMT-4321 (NANOMAGCOST-CM) and by the Spanish MICINN Projects RTI2018-097895-B-C42 (FUN-SOC), PID2021-122980OB-C52 (ECLIPSE-ECoSOx) and the "Severo Ochoa" Programme for Centres of Excellence in R&D (CEX2020-001039-S). S.B. acknowledges funding from Deutsche Forschungsgemeinschaft (DFG) through the Collaborative Research Center SFB 1238 (Project No. C01). G.B. gratefully acknowledges the computing time granted through JARA-HPC on the supercomputer JURECA at Forschungszentrum Jülich.

Open Access Funding provided by Elettra Sincrotrone Trieste SCpA within the CRUI-CARE Agreement.

Conflict of Interest

The authors declare no conflict of interest.

Data Availability Statement

The data that support the findings of this study are available from the corresponding author upon reasonable request.

Keywords

graphene, rare-earth elements, spin-polarized flat bands, spin–orbit coupling

Received: February 14, 2023
Revised: March 27, 2023
Published online: July 21, 2023

[1] M. Kang, S. Fang, L. Ye, H. C. Po, J. Denlinger, C. Jozwiak, A. Bostwick, E. Rotenberg, E. Kaxiras, J. G. Checkelsky, R. Comin, *Nat. Commun.* **2020**, *11*, 4004.
[2] K. Sun, Z. Gu, H. Katsura, S. D. Sarma, *Phys. Rev. Lett.* **2011**, *106*, 236803.
[3] Z. Liu, F. Liu, Y.-S. Wu, *Chin. Phys. B* **2014**, *23*, 077308.
[4] N. B. Kopnin, T. T. Heikkilä, G. E. Volovik, *Phys. Rev. B* **2011**, *83*, 220503.
[5] D. Leykam, A. Andreanov, S. Flach, *Adv. Phys. X* **2018**, *3*, 1473052.
[6] B. Hunt, J. D. Sanchez-Yamagishi, A. F. Young, M. Yankowitz, B. J. LeRoy, K. Watanabe, T. Taniguchi, P. Moon, M. Koshino, P. Jarillo-Herrero, R. C. Ashoori, *Science* **2013**, *340*, 1427.
[7] C. R. Dean, L. Wang, P. Maher, C. Forsythe, F. Ghahari, Y. Gao, J. Katoch, M. Ishigami, P. Moon, M. Koshino, T. Taniguchi, K. Watanabe, K. L. Shepard, J. Hone, P. Kim, *Nature* **2013**, *497*, 598.
[8] L. A. Ponomarenko, R. V. Gorbachev, G. L. Yu, D. C. Elias, R. Jalil, A. A. Patel, A. Mishchenko, A. S. Mayorov, C. R. Woods, J. R. Wallbank, M. Mucha-Kruczynski, B. A. Piot, M. Potemski, I. V. Grigorieva, K. S. Novoselov, F. Guinea, V. I. Fal'ko, A. K. Geim, *Nature* **2013**, *497*, 594.
[9] J. C. W. Song, A. V. Shytov, L. S. Levitov, *Phys. Rev. Lett.* **2013**, *111*, 266801.
[10] R. Bistritzer, A. H. MacDonald, *Proc. Natl. Acad. Sci. USA* **2011**, *108*, 12233.
[11] Y. Cao, V. Fatemi, A. Demir, S. Fang, S. L. Tomarken, J. Y. Luo, J. D. Sanchez-Yamagishi, K. Watanabe, T. Taniguchi, E. Kaxiras, R. C. Ashoori, P. Jarillo-Herrero, *Nature* **2018**, *556*, 80.
[12] A. H. Castro Neto, F. Guinea, N. M. R. Peres, K. S. Novoselov, A. K. Geim, *Rev. Mod. Phys.* **2009**, *81*, 109.
[13] J. Liu, X. Dai, *Nat. Rev. Phys.* **2021**, *3*, 367.
[14] F. R. Geisenhof, F. Winterer, A. M. Seiler, J. Lenz, T. Xu, F. Zhang, R. T. Weitz, *Nature* **2021**, *598*, 53.
[15] S. Link, S. Forti, A. Stöhr, K. Küster, M. Rösner, D. Hirschmeier, C. Chen, J. Avila, M. C. Asensio, A. A. Zakharov, T. O. Wehling, A. I. Lichtenstein, M. I. Katsnelson, U. Starke, *Phys. Rev. B* **2019**, *100*, 121407.
[16] L. Classen, A. V. Chubukov, C. Honerkamp, M. M. Scherer, *Phys. Rev. B* **2020**, *102*, 125141.
[17] P. Rosenzweig, H. Karakachian, D. Marchenko, K. Küster, U. Starke, *Phys. Rev. Lett.* **2020**, *125*, 176403.
[18] N. Ehlen, M. Hell, G. Marini, E. H. Hasdeo, R. Saito, Y. Falke, M. O. Goerbig, G. Di Santo, L. Petaccia, G. Profeta, A. Grüneis, *ACS Nano* **2020**, *14*, 1055.
[19] M. Jugovac, C. Tresca, I. Cojocariu, G. Di Santo, W. Zhao, L. Petaccia, P. Moras, G. Profeta, F. Bisti, *Phys. Rev. B* **2022**, *105*, L241107.
[20] S.-H. Lee, Y. Kim, B. Cho, J. Park, M.-S. Kim, K. Park, H. Jeon, M. Jung, K. Park, J. Lee, J. Seo, *Commun. Phys.* **2022**, *5*, 235.
[21] M. Li, Q. Wang, G. Wang, Z. Yuan, W. Song, R. Lou, Z. Liu, Y. Huang, Z. Liu, H. Lei, Z. Yin, S. Wang, *Nat. Commun.* **2021**, *12*, 3129.
[22] N. Regnault, Y. Xu, M.-R. Li, D.-S. Ma, M. Jovanovic, A. Yazdani, S. S. P. Parkin, C. Felser, L. M. Schoop, N. P. Ong, R. J. Cava, L. Elcoro, Z.-D. Song, B. A. Bernevig, *Nature* **2022**, *603*, 824.
[23] K. S. Novoselov, V. I. Fal'ko, L. Colombo, P. R. Gellert, M. G. Schwab, K. Kim, *Nature* **2012**, *490*, 192.
[24] K. S. Novoselov, A. K. Geim, S. V. Morozov, D. Jiang, Y. Zhang, S. V. Dubonos, I. V. Grigorieva, A. A. Firsov, *Science* **2004**, *306*, 666.
[25] N. Rougemaille, A. T. N'Diaye, J. Coraux, C. Vo-Van, O. Fruchart, A. K. Schmid, *Appl. Phys. Lett.* **2012**, *101*, 142403.
[26] M. Blanco-Rey, P. Perna, A. Gudin, J. M. Diez, A. Anadón, P. Olleros-Rodríguez, L. de Melo Costa, M. Valvidares, P. Gargiani, A. Guedeja-Marron, M. Cabero, M. Varela, C. García-Fernández, M. M. Otrokov, J. Camarero, R. Miranda, A. Arnau, J. I. Cerdá, *ACS Appl. Nano Mater.* **2021**, *4*, 4398.
[27] F. Ajejas, A. Anadon, A. Gudin, J. M. Diez, C. G. Ayani, P. Olleros-Rodríguez, L. de Melo Costa, C. Navío, A. Gutierrez, F. Calleja, A. L. Vázquez de Parga, R. Miranda, J. Camarero, P. Perna, *ACS Appl. Mater. Interfaces* **2020**, *12*, 4088.
[28] H. Yang, A. D. Vu, A. Hallal, N. Rougemaille, J. Coraux, G. Chen, A. K. Schmid, M. Chshiev, *Nano Lett.* **2016**, *16*, 145.

[29] H. Yang, G. Chen, A. A. C. Cotta, A. T. N'Diaye, S. A. Nikolaev, E. A. Soares, W. A. A. Macedo, K. Liu, A. K. Schmid, A. Fert, M. Chshiev, *Nat. Mater.* **2018**, *17*, 605.
[30] F. Ajejas, A. Gudín, R. Guerrero, A. Anadón Barcelona, J. M. Diez, L. de Melo Costa, P. Olleros, M. A. Niño, S. Pizzini, J. Vogel, M. Valvidares, P. Gargiani, M. Cabero, M. Varela, J. Camarero, R. Miranda, P. Perna, *Nano Lett.* **2018**, *18*, 5364.
[31] B. M. Cano, A. Gudín, J. Sánchez-Barriga, O. J. Clark, A. Anadón, J. M. Díez, P. Olleros-Rodríguez, F. Ajejas, I. Arnay, M. Jugovac, J. Rault, P. L. Févre, F. Bertran, D. Mazhjoo, G. Bihlmayer, S. Blügel, R. Miranda, J. Camarero, M. A. Valbuena, P. Perna, arxiv:2206.04351 **2022**.
[32] A. Anadón, A. Gudín, R. Guerrero, I. Arnay, A. Guedeja-Marron, P. Jiménez-Cavero, J. M. Díez Toledano, F. Ajejas, M. Varela, S. Petit-Watelot, I. Lucas, L. Morellón, P. A. Algarabel, M. R. Ibarra, R. Miranda, J. Camarero, J. C. Rojas-Sánchez, P. Perna, *APL Mater.* **2021**, *9*, 061113.
[33] F. Huttmann, D. Klar, N. Atodiresei, C. Schmitz-Antoniak, A. Smekhova, A. J. Martínez-Galera, V. Caciuc, G. Bihlmayer, S. Blügel, T. Michely, H. Wende, *Phys. Rev. B* **2017**, *95*, 075427.
[34] P. Gargiani, R. Cuadrado, H. B. Vasili, M. Pruneda, M. Valvidares, *Nat. Commun.* **2017**, *8*, 699.
[35] T. Jungwirth, X. Marti, P. Wadley, J. Wunderlich, *Nat. Nanotechnol.* **2016**, *11*, 231.
[36] M. Jugovac, F. Genuzio, E. Gonzalez Lazo, N. Stojić, G. Zamborlini, V. Feyer, T. O. Menteş, A. Locatelli, C. M. Schneider, *Carbon* **2019**, *152*, 489.
[37] M. Jugovac, E. D. Donkor, P. Moras, I. Cojocariu, F. Genuzio, G. Zamborlini, G. Di Santo, L. Petaccia, N. Stojić, V. Feyer, C. M. Schneider, A. Locatelli, T. O. Menteş, *Carbon* **2022**, *198*, 188.
[38] M. Jugovac, *Ph.D. Thesis*, University of Duisburg-Essen, Duisburg/Essen, Germany, **2020**.
[39] D. Marchenko, A. Varykhalov, J. Sánchez-Barriga, O. Rader, C. Carbone, G. Bihlmayer, *Phys. Rev. B* **2015**, *91*, 235431.
[40] S. Schumacher, F. Huttmann, M. Petrović, C. Witt, D. F. Förster, C. Vo-Van, J. Coraux, A. J. Martínez-Galera, V. Sessi, I. Vergara, R. Rückamp, M. Grüninger, N. Schleheck, F. Meyer zu Heringdorf, P. Ohresser, M. Kralj, T. O. Wehling, T. Michely, *Phys. Rev. B* **2014**, *90*, 235437.
[41] S. Sung, S. Kim, P. Lee, J. Kim, M. Ryu, H. Park, K. Kim, B. I. Min, J. Chung, *Nanotechnology* **2017**, *28*, 205201.
[42] C. Wiemann, M. Patt, I. P. Krug, N. B. Weber, M. Escher, M. Merkel, C. M. Schneider, *e-J. Surf. Sci. Nanotechnol.* **2011**, *9*, 395.
[43] C. Tusche, M. Ellguth, A. Krasyuk, A. Winkelmann, D. Kutnyakhov, P. Lushchyk, K. Medjanik, G. Schönhense, J. Kirschner, *Ultramicroscopy* **2013**, *130*, 70.
[44] J. E. Prieto, O. Krupin, S. Gorovikov, K. Döbrich, G. Kaindl, K. Starke, *Phys. Rev. B* **2005**, *72*, 092409.
[45] J. P. Perdew, K. Burke, M. Ernzerhof, *Phys. Rev. Lett.* **1996**, *77*, 3865.
[46] S. Grimme, J. Antony, S. Ehrlich, H. Krieg, *J. Chem. Phys.* **2010**, *132*, 154104.
[47] H. Krakauer, M. Posternak, A. J. Freeman, *Phys. Rev. B* **1979**, *19*, 1706.
[48] FLEUR, a full-potential linearized augmented planewave code based on density-functional theory, https://www.flapw.de.